

# The X-ray Iron Emission from Tycho’s Supernova Remnant

Una Hwang<sup>1,2</sup>, John P. Hughes<sup>3</sup>, & Robert Petre<sup>1</sup>

## ABSTRACT

We present the results of broadband spectral model fits to the X-ray spectrum of Tycho’s supernova remnant obtained by the Solid-State Imaging Spectrometers on the ASCA Observatory. We use single-temperature, single-ionization-age, nonequilibrium ionization models to characterize the ejecta and the blast-shocked interstellar medium. Previous spectral studies have suggested that the Fe ejecta in this Type Ia remnant are stratified interior to the other ejecta. These studies, however, have generally restricted their attention to the Fe K blend at 6.5 keV. ASCA provides data over a broad energy range that allow the placement of important constraints simultaneously from the Fe L emission near 1 keV as well as the Fe K emission. We find that the simplest models, with emission from the ejecta and blast wave each at a single temperature and ionization age, severely underestimate the flux in the Fe K blend. These models also show that there is little Fe emission associated with the Si and S ejecta shell, which has an average temperature  $kT \sim 0.86$  keV and ionization age  $n_e t \sim 10^{11}$  cm<sup>-3</sup> s. The blast-shocked interstellar medium has abundances roughly 0.3 times the solar value, while the ejecta, with the exception of Fe, have relative abundances that are typical of Type Ia supernovae. The addition of another component of Fe emission, which we associate with ejecta, at a temperature at least two times higher and an ionization age  $\sim 100$  times lower than the Si ejecta, does provide a good fit to the spectrum. This model is consistent with imaging results. Although fluorescent emission from dust in the remnant may contribute to the Fe K flux, we conclude that it is unlikely to be the dominant component.

*Subject headings:* ISM: supernova remnants—Xrays: interstellar medium

---

<sup>1</sup>NASA Goddard Space Flight Center, Laboratory for High Energy Astrophysics, Greenbelt, MD 20771

<sup>2</sup>Department of Astronomy, University of Maryland at College Park, MD 20742

<sup>3</sup>Department of Physics and Astronomy, Rutgers University, P.O. Box 849, Piscataway, NJ 08855

## 1. Introduction

An important issue concerning supernova ejecta is whether or not the radially distributed layers formed during hydrostatic and explosive nucleosynthesis are preserved, or if these layers are mixed together. According to models of Type Ia supernovae (explosive accretion-induced burning instabilities in white dwarfs), the ejecta are expected to retain some of their stratification (e.g., Nomoto et al. 1984). Although the outer layers of the ejecta may be mixed by convective instabilities, as is suggested by the early-time spectra of Type Ia supernovae (Branch et al. 1985), the Fe ejecta may remain distinct from other ejecta in an inner layer, and thus be only partially heated by the reverse shock. This scenario is supported by UV observations of the supernova remnant SN1006 (Wu et al. 1983, 1993, 1997). Absorption due to cold Fe is observed in the continuum emission from a background star, providing evidence for the presence of unshocked Fe ejecta in the interior of the remnant. By contrast, observations of SN 1987a show that the ejecta are evidently well-mixed in the remnants of supernovae caused by the gravitational collapse of massive progenitors (Type II, Ib, and Ic; Woosley 1991 and references therein).

The remnant of the supernova recorded by Tycho Brahe in 1572 is generally considered to be the prototype of Type Ia remnants. It has been studied extensively at all wavelengths, but information about its ejecta can now be obtained only from its X-ray emission. The optical emission from this young remnant is virtually all H Balmer emission due to the excitation of partially neutral ambient material at the outer shock wave (Smith et al. 1991). Even in remnants with bright optical emission from the ejecta, the mass of optically emitting material represents only a tiny fraction of the total ejecta mass; X-rays are the dominant emission at the characteristic temperature of the shock-heated material which comprises a supernova remnant (SNR). Hamilton, Sarazin, & Szymkowiak (1986) were the first to suggest that much of the Fe ejecta could be hidden in an inner layer. They applied a self-similar hydrodynamical model for the ejecta in Tycho to a number of observations over a wide range of energies. In their model, a small amount of Fe ejecta mixed together with Si and other ejecta provide most of the X-ray emission from Fe; the inner layers of Fe are too cool to provide significant X-ray emission. A number of other spectral studies suggest that the Fe ejecta are stratified interior to the lighter ejecta. Hughes (1991) and Petre et al. (1992) showed that the centroid of the Fe K blend requires a significantly lower ionization age than the other elements. The ionization age is defined as  $n_e t$ , the product of electron density with time since the gas was shock-heated. Because remnants are low-density plasmas (electron density  $n_e \sim 1 \text{ cm}^{-3}$ ), the time required to attain the equilibrium population distribution of ions at a given temperature ( $\sim 10^4/n_e \text{ yr}$ ) generally exceeds the age of the remnant. The low ionization age of the Fe emission could be interpreted as evidence for the stratification of Fe ejecta within interior layers of the remnant that have only recently been heated by the reverse shock. However, another possibility is that the Fe K emission arises in lower density ambient material shocked by the blast wave.

More recent observations with the ASCA Solid State Imaging Spectrometers (SIS) have now provided a superior moderate resolution spectrum of Tycho’s SNR at energies between 0.4–10 keV

with 1' spatial resolution. Hwang & Gotthelf (1997; hereafter HG97) use these data in a study of the line emission. Using measured emission line intensity ratios and centroids of emission line blends, they conclude with other authors that the Fe emission arises under conditions different from Si and S, namely a higher temperature and lower ionization age. Their narrowband ASCA images also show that the spatial distributions of Fe L and Fe K emission are not the same. The Fe K emission is somewhat more centrally distributed than all other X-ray spectral features distinguishable by ASCA. This central distribution of the Fe K emission suggests that it may arise from hot inner ejecta layers and not from the blast wave.

As suggestive as this evidence is, the nature of the Fe emission in Tycho's SNR merits a more careful inquiry. A difference between the average spectral properties of the elements Si and Fe does not necessarily require that they be spatially separate. A range of temperatures coupled with the corresponding differences in emissivity for different ions could allow them to occupy the same volume, with the Si emission dominating at the lower temperatures and the Fe emission at higher temperatures. The X-ray spectrum is also clearly complex, and emission from the blast-shocked interstellar medium is expected to make a contribution. High resolution images from the Einstein Observatory (Seward, Gorenstein, & Tucker 1983) resolve a thin shelf of emission attributed to the blast wave, which is estimated to contribute 28% of the counts in the Einstein energy bandpass (0.5–4.5 keV). Instruments with sensitivity at higher energies have also clearly detected harder X-ray emission (Pravdo & Smith 1979, Fink et al. 1994). Model fitting is therefore necessary.

With the exception of the hydrodynamic similarity model of HSS86, the results presented so far in support of the stratification of the Fe ejecta are based on the line diagnostics approach of comparing measured emission line intensities and centroids to theoretical models. They have focused on the centroid of the Fe K blend, assuming that this emission is from the ejecta, and at best make rough comparisons of the Fe L and Fe K intensities (Vancura, Gorenstein, & Hughes 1995 and HG97). This is because the Fe L emission at energies near 1 keV is inaccessible to line diagnostics with data obtained by ASCA and all previous X-ray broadband spectrometers. The numerous line transitions that are collectively referred to as Fe L are blended together by the ASCA spectrometers, and individual Fe L line intensities cannot be measured relative to the continuum. Fitting a model to the broadband spectrum allows us to maximize our use of the spectral data, particularly the Fe L emission.

In this paper we use the ASCA SIS spectral data to investigate further the nature of the Fe emission by carrying out broadband model fits including nonequilibrium ionization (NEI) effects. We use single-temperature, single-ionization age NEI models to represent both the ejecta and the blast-shocked interstellar medium. We build on the results of HG97 by using their results for the temperature of the Si ejecta. The shape and intensity of the Fe L emission at energies near 1 keV provide critical constraints on these models.

## 2. Procedure and Results

The characteristics of the ASCA SIS and our data reduction procedures are described in HG97 and the references therein. Briefly, the SIS consists of two slightly misaligned square arrays of 4 CCD chips, each with its own telescope. The telescope provides imaging with a narrow  $1'$  core and extended wings with a half-power diameter of  $3'$ . Each SIS can be operated with 1, 2, or all 4 of its chips exposed. Spectra are obtained over energies of 0.4–10 keV with a spectral resolution of 2% at 6 keV (resolution at launch) that scales with energy like  $E^{-1/2}$ . The data for Tycho’s SNR were taken in 2- and 4-CCD mode on 29 August 1993 during the Performance Verification phase of the mission. In this paper, we use only the spectral data taken in 2-CCD mode to minimize the impact of calibration uncertainties, which are significantly greater for data taken in 4-CCD mode. Because Tycho is so bright in X-rays, its spectrum is particularly sensitive to such uncertainties. We study in detail the spectrum obtained by the best-calibrated CCD chip (chip 1 on SIS0), which covers roughly the southeastern quadrant of the remnant. The ASCA spectrum of Tycho’s SNR shows only relatively modest variations with position (HG97).

Line widths are clearly in excess of the predicted instrumental widths. We find that a Gaussian broadening corresponding to a velocity of about  $7500 \text{ km s}^{-1}$  FWHM is adequate for all the emission lines. This cannot be considered a measurement of physical velocities in the remnant: the instrumental response is not yet perfectly understood, and some percentage of this width is probably attributable to imperfect calibration.

### 2.1. Spectral Fits

In our models we include the emission from the blast-shocked interstellar medium (ISM) and the reverse-shocked ejecta, representing each by a single-temperature, single-ionization-age, NEI component. Although this approach sounds simple, Hamilton & Sarazin (1984) have shown that many commonly-invoked hydrodynamic scenarios relevant to supernova remnants can be well-approximated with an emission-averaged temperature and ionization parameter. To first order, the reverse shock and blast shock should each be characterizable in this way.

Such a model, however, cannot be a perfect representation of an object as complex as a young supernova remnant. The X-ray emitting gas in remnants has a distribution of temperatures and densities arising from their complex hydrodynamic evolution. Our goals are to characterize as simply as possible the emission-weighted average properties of the important contributions to the X-ray spectrum. With this approach, one is not constrained *a priori* to an explicit hydrodynamic model. An important advantage is that the reduced computational burden allows us to explore a wider range of parameter space. This approach has been applied successfully in the past to study other supernova remnants (e.g., Hughes & Singh 1994, Hwang et al. 1993).

The spectral fits employ the X-ray thermal emission models of Raymond & Smith (1977,

with updates 1992) with the calculation of the nonequilibrium ionization fractions carried out using matrix diagonalization techniques (Hughes & Helfand 1985). The NEI code uses ionization and recombination rates from the basic Raymond & Smith code to calculate the time-dependent ionization state of gas which has been impulsively heated to a high temperature by the passage of a shock wave. Additional lines appropriate to the NEI situation have also been added to the model using data from Mewe, Gronenschild, & van den Oord (1985), as explained in Hughes & Singh (1994). See this reference for further discussion of NEI effects on X-ray spectra. In our fits, the abundances of the elements are quoted relative to the solar values of Allen (1973; Fe/H =  $3.98 \times 10^{-5}$  by number).

In the following three sections, we present fits of models with one, two, and three NEI components.

## 2.2. Against a Blast Wave Origin for the Fe K Emission

HG97 report a temperature  $kT$  of about 0.86 keV and an ionization age  $n_e t$  of about  $10^{11} \text{ cm}^{-3} \text{ s}$  for the Si and S ejecta based on their analysis of the emission line intensity ratios. These and other authors note that there is additional emission at energies above about 5 keV. To better characterize this hard emission, we first fitted the spectrum at energies above 4.5 keV with a NEI component for Fe and Ni and an additional component from H and He at the same temperature providing most of the continuum emission; the abundances of Fe and Ni were required to be the same. At energies above 4.5 keV, the 0.86 keV ejecta component contributes very little to the spectrum.

The fits were performed for a grid of temperatures  $kT$  from 2.5 to 20 keV, as summarized in Table 1. The ionization age is about  $10^{10} \text{ cm}^{-3} \text{ s}$  for the entire range of temperatures, and the abundance required to reproduce the Fe K line intensity is 1.5–3.5 times the solar value; at a temperature  $kT = 20 \text{ keV}$ , the lower limit for the abundance ( $\Delta\chi^2 = 2.71$ ) is consistent with the solar value. The high abundances required suggest that the Fe K emission cannot come primarily from a blast wave in the interstellar medium unless the ISM is significantly enriched in this region. There is no independent evidence for such enrichment, however. Furthermore, extrapolation of the best-fit model ( $kT = 4.5 \text{ keV}$ ) throughout the entire ASCA band shows that this model cannot be correct (Figure 1). With the H absorption column density fixed at the nominal Galactic value of  $4.5 \times 10^{21} \text{ cm}^{-2}$  (Albinson et al. 1986), the Fe L emission is severely overpredicted, even in the absence of the  $kT = 0.86 \text{ keV}$  ejecta component required to explain the strong Si and S emission. Any reasonable increase in the column density cannot make the model consistent with the data.

We may also consider whether a Sedov-type blast wave yields the required intensity in the Fe K blend. The age is known to be 421 yr at the time of the ASCA observations. An ambient H density of about  $0.3 \text{ cm}^{-3}$  is estimated by both Seward et al. (1983) and Kirshner et al. (1987) from X-ray and optical observations, respectively. The width of the broad H Balmer lines in the

optical give a blast wave velocity of 1500–2800 km s<sup>-1</sup> (Smith et al. 1991). For a distance of 2.3 kpc to Tycho (Green 1984), the optical and radio proper motion studies give blast wave velocities consistent with this. The X-ray proper motion study using the ROSAT HRI by Hughes (1996) shows two velocity components: the lower velocity is consistent with the radio and optical values, but the higher velocity, presumably associated with the blast wave, is about  $4600 \pm 1400$  km s<sup>-1</sup> for a distance of 2.3 kpc. For our calculation we use the optical velocity since it is independent of distance, but note that the optical velocities may not be representative of the average shock velocity. Reynolds et al. (1996) and Hughes (1996) report significant variation in the velocity around the rim of the remnant in the radio and in X-rays, respectively. Our conclusions do not change if we adopt the higher X-ray determined blast velocity.

Using the equations given in Hamilton, Sarazin, & Chevalier (1983), we derive the shock temperature as  $kT = 2.8\text{--}9.6$  keV and the ionization parameter  $\log \eta \equiv n_o^2 E$  (erg cm<sup>-6</sup>) = 47.8–49.1, where  $n_o$  is the ambient H density in cm<sup>-3</sup> and  $E$  is the explosion energy in 10<sup>51</sup> ergs. For these values, the predicted flux in Fe K from a solar abundance plasma is more than an order of magnitude lower than that measured by ASCA, and the predicted equivalent width is at least several times too low. Therefore, in the context of a Sedov model, the observed Fe K emission requires the ambient Fe abundance to be several times higher than the solar value.

Based on the foregoing, we conclude that while emission from the blast wave may provide most of the continuum at energies above 5 keV, it cannot provide the bulk of the Fe K line emission. At the temperature required to model the continuum, and the ionization age required to reproduce the Fe K blend at the observed energy, this model cannot provide sufficient flux in the Fe K emission without severely overpredicting the Fe L emission. We proceed, nevertheless, to fit the data with two NEI components representing the ejecta and the blast wave in order to gain insights concerning the shape of the overall spectrum, the relative abundances of the elements in the ejecta, and the abundances in the blast-shocked ISM.

### 2.3. Fits for Ejecta and Blast Components

In these fits, the ejecta component is fixed at a temperature of  $kT = 0.86$  keV following HG97. All the important elements are included in this component, with He, C, and N in their solar abundance ratios relative to H, the O abundance tied to that of Ne, and Fe tied to Ni. The abundances of O, Mg, Si, S, Ar, Ca, and Fe are therefore fitted freely, as are the ionization parameter and the absorbing interstellar H column density. For the blast wave component, the element abundances are assumed to be in their solar ratios. We fitted the data at energies from 0.6–10 keV to avoid the oxygen edge in the detector response at 0.54 keV.

All the fitted models are conspicuously deficient in emission at energies near 0.7 and 1.2 keV. We have also noticed this effect when fitting other supernova remnant spectra using this NEI model and believe that this is most likely due to incompleteness in the lines included in the

models or inaccuracies in the atomic physics used. Liedahl, Osterheld, & Goldstein (1995) have recalculated Fe L emissivities for the Fe 23 and Fe 24 ions and find some significant deficiencies in the Fe L emissivities at energies near 1.1 keV in the current Raymond & Smith code. This may partially explain the deficit in our fits at 1.2 keV; it certainly highlights the need for updated atomic calculations. We therefore included two gaussian emission lines at approximately 0.726 and 1.200 keV in the models, with equivalent widths of 200–300 eV and 60–80 eV, respectively. We assume that these features are Fe lines. The Raymond & Smith model has features due to Fe 16 (0.725 keV) and Fe 17 (0.727 keV), and Fe 20 (1.204 keV) and Ni 24 (1.204 keV) at approximately these energies<sup>4</sup>.

The results of the fits for a grid of blast-wave temperatures  $kT$  ranging from 2.5 to 20 keV are given in Table 2. The minimum  $\chi^2$  is obtained for a blast temperature  $kT = 3.6$  keV. The fitted column density of  $5.7 \times 10^{21} \text{ cm}^{-2}$  is slightly higher than the nominal Galactic value measured in the radio (Albinson et al. 1986), and is high enough to result in significant attenuation of the X-ray spectrum at energies below 0.8 keV. The abundance of Fe in the ejecta component is low, showing that there is little Fe associated with the gas emitting the Si and S lines. Allowing a separate ionization age for Fe at the same temperature as Si does not significantly alter the fitted Fe abundance. The Fe L emission at energies near 1 keV is very weak, and determines the Fe abundance in the ejecta component at a temperature  $kT = 0.86$  keV and ionization age  $n_e t \sim 10^{11} \text{ cm}^{-3} \text{ s}$ ; such gas is too cool to contribute significantly to the Fe K emission. The dominant Fe ions are Fe 19 and Fe 20. The weakness of the Fe L emission also imposes subsolar abundances for the blast component (see Table), resulting in a strong deficit in the Fe K blend emission in the models as expected from the results of the preceding section. This is illustrated in Figure 2, which shows the best-fit model with temperatures  $kT = 0.86$  (ejecta) and 3.6 keV (blast), folded through the instrument response and overlaid on the data. The contribution to the spectrum from the ejecta and blast components are also shown separately.

Only the Si and Fe abundances are listed in Table 2 for the  $kT = 0.86$  keV ejecta component. In Figure 3, we compare the ratios of the abundances of the elements O (tied to Ne), Mg, S, Ar, Ca, and Fe in this component to that of Si, relative to the solar values of Allen (1973), for the entire set of fits in Table 2. The relative abundances of the intermediate mass elements Si, S, Ar, and Ca vary by less than 50% over the entire range of temperatures; the abundances of O, Mg, and Fe vary somewhat more. Shown in the same figure are the predicted abundances of these elements relative to Si relative to the solar abundances of Allen (1973) in the W7 model for a Type Ia supernova of Nomoto et al. (1984) and the updated calculations of Thielemann et al. (1993). Our fitted abundances for Si, S, Ar, and Ca are in good qualitative agreement with the Nomoto et al. results; the newer calculations predict a lower Ca mass, which makes Ca/Si about a factor three

---

<sup>4</sup>Between 0.70–0.74 keV, the model includes lines of Ca 16 (0.708 keV), Fe 16 (0.708, 0.725 keV) and Fe 17 (0.727, 0.739 keV); between 1.200–1.230 keV, the model includes lines of Ne 10 (1.211 keV), Fe 20 (1.204 keV), and Ni 19 (1.228 keV), Ni 24 (1.204 keV), and Ni 25 (1.216 keV).

lower than in our fits. It should be noted here that the high abundance of Ca relative to Fe makes the Ca L shell emission important at energies near 0.7 keV and below. The Ca abundance may be constrained more by this part of the spectrum than by the Ca K blend, but the L-shell atomic physics are probably not as reliable as that for the K-shell (cf. Liedahl et al. 1995). The influence of the Ca L shell lines may also be responsible for the line energy of the Ca K blend at energy  $\sim 4.9$  keV appearing to be slightly too high relative to the data. Alternatively, the ionization age for Ca may actually be different from that for Si and S.

The results in Table 2 also show that the fitted ionization age  $n_e t$  for the hotter component is near  $10^{10} \text{ cm}^{-3} \text{ s}$  for the entire range of temperatures considered. The ionization age is determined primarily by the shape of the Fe L emission, and its value indicates that Fe 17–19 are the dominant Fe ions in this component. The constancy of the fitted ionization age with temperature shows that the discrepancy between the Fe L and K intensities cannot be resolved with a multi-temperature plasma with temperatures between 2.5 and 20 keV unless a range of ionization ages is also invoked.

The additional Fe K emission evidently comes from a component that does not contribute significantly to the Fe L emission, as the spectrum is well-fit everywhere by a two-component model except at the Fe K blend. We consider two possibilities in the following sections: Fe ejecta which are stratified interior to the other ejecta and therefore at a different temperature and ionization age, and fluorescent Fe K emission from Fe in dust grains, as was recently proposed by Borkowski & Szymkowiak (1997).

## 2.4. Stratified Fe Ejecta

In this section, we consider fit results for an ejecta component at temperature  $kT = 0.86$  keV, a blast component at temperature  $kT = 4$  keV, and an additional Fe emission component that we associate with ejecta. The results of these fits are given in Table 3 for a range of temperatures from 1–20 keV for the Fe ejecta. Again, only the Si and Fe abundances are given in the table for the 0.86 keV component, but the abundances for the other elements relative to Si are similar to those in the two-component fits of the previous section.

The lower limit of the Fe temperature is about twice the temperature of the Si ejecta. We do not attempt to constrain the upper limit of the Fe ejecta temperature. The Fe K centroid energy changes only gradually with temperature above about  $kT = 1.5$  keV, so good fits can be obtained at all these temperatures. As the temperature of the Fe ejecta is allowed to increase above the temperature of the blast wave, the formal  $\chi^2$  continues to decrease gradually. The ionization age of the Fe ejecta is roughly 100 times lower than the ionization age of the Si ejecta, so that the dominant Fe ions are in low ionization stages: Fe 10–12, if their temperature is about 1.6 keV, or Fe 14–17, if their temperature is as high as 20 keV. The low ionization age of the Fe ejecta component suggests that the Fe ejecta were more recently shocked than the Si ejecta, and had expanded to lower densities. The exact translation from an average ionization age to density

is complicated, however, because the ejecta are made of pure heavy elements and the electron population evolves with time as the metals are gradually ionized.

The temperature of the blast wave in this situation is somewhat uncertain. We have fixed it to a value of 4.0 keV, which is between the best fit temperature of 4.5 keV in the one-temperature NEI fits and the best fit temperature of 3.6 keV in the two-temperature NEI fits. Because we have obtained a good fit for the parameters chosen, and in light of the computational load required to search the entire parameter space, we have not explored the full range of possible blast wave temperatures. This should be borne in mind. Fits with blast temperatures of 3.0, 3.5, or 4.5 keV were generally statistically comparable to those with blast temperatures of 4.0 keV ( $\Delta\chi^2$  within 2.7).

Figure 4 shows the model with the Fe ejecta at temperature  $kT = 1.6$  keV and the blast wave at temperature  $kT = 4$  keV. As can be seen, the fit is much improved over Figure 2, both formally, and to the eye. From the figure, it is seen that the blast wave contributes most of the emission in the Fe L region at energies between 0.7–1.0 keV. The line emission makes up 56% of the total count rate in the Fe K band. The blast wave component contributes 14% of the observed count rate in the Fe K line with an energy of 6.50 keV; the Fe ejecta at temperature  $kT = 1.6$  keV contribute 70% of the count rate in the line with an energy of 6.41 keV. We will address the remaining 16% not accounted for by the model in the discussion section.

## 2.5. Dust Depletion and Fluorescence of Fe

HG97 note that a possible alternative explanation for the low ratio of Fe L to Fe K intensity is offered by Borkowski & Szymkowiak (1997; hereafter BS97), who point out that collisionally-excited Fe in dust grains will fluoresce efficiently in the K transitions, but not the L transitions. If Fe is depleted onto dust grains, this results in a low Fe L/Fe K intensity ratio: all the Fe line intensities are decreased because the Fe is depleted onto dust, but the Fe K intensity is supplemented by fluorescent emission from the Fe in dust grains, while the Fe L intensity is not. As noted by BS97, this is a plausible scenario when dust is present in the remnant and the ionization age is low enough that the observed Fe K line energy is near 6.4 keV, the energy of the transition in neutral Fe. Dust is clearly present in Tycho, as is evidenced by its IR emission (Braun 1987). The fitted energy centroid of the Fe K blend in data from the best-calibrated ASCA CCD chip (SIS0, chip 1) is 6.471 (6.444–6.500,  $\Delta\chi^2 = 2.71$ ). The systematic error in the line energy must be taken to be its nominal value of 0.5%, or about 0.03 keV for a line energy of 6.4 keV. There is unfortunately no independent way to set the energy scale for Tycho’s ASCA spectrum, as there are no strong unblended lines at known energies. Given the errors, the centroid of the Fe K emission in Tycho is low enough that fluorescent K emission from neutral Fe could be important.

We use the calculations of BS97 for the emissivity of a dusty gas of Fe to calculate the mass of Fe required to reproduce Tycho’s Fe K flux. The top panel of Figure 2 in BS97 plots the Fe

K centroid as a function of ionization age at the temperatures  $kT = 1, 2,$  and  $10$  keV. These calculations are carried out assuming (1) no dust and (2) an initial depletion of 95% of the Fe onto dust. For temperatures other than these, we interpolate between the calculations. From the measured Fe K centroid, the ionization age  $n_e t$  is  $\sim 10^{10}$  cm $^{-3}$  s in gas without dust, which agrees well with the NEI fits for the Fe K region in Table 1. The ionization age can be as high as  $n_e t \sim 10^{10.3}$  cm $^{-3}$  s in gas with dust, depending on the temperature. Having set the ionization age to be  $10^{10.3}$  cm $^{-3}$  s for the dusty gas, we then use the measured Fe K flux of  $4.4 \times 10^{-4}$  photons cm $^{-2}$  s $^{-1}$  from HG97 together with emissivities plotted in Figure 1 of BS97 to deduce the Fe masses given in Table 4. These represent the total mass of Fe in both gas and dust. We can estimate how much of this mass is in gas by using the fitted emission measures and abundances for the blast-shocked component from our two-temperature fits (Table 2). These masses are also given in the table. The implied mass of Fe in dust is between  $0.002 M_\odot$ , if  $kT = 10$  keV for the blast wave, and  $0.017 M_\odot$ , if  $kT = 2.5$  keV. The calculations assume a spherical shell of thickness  $1/10$  the radius and a distance of 2.3 kpc to Tycho’s SNR (Green 1984).

These mass calculations can be compared to the estimated mass in the dust from the IRAS observations. Braun (1987) estimates that the mass of dust is  $0.008 M_\odot$  based on the IR brightness distribution and intensity for a distance of 2.3 kpc. For solar abundance ratios and a mixture of graphite and silicate grains, about  $0.002 M_\odot$  of this dust mass is Fe. This is much lower than the dust masses in Table 4 at all temperatures below  $kT = 10$  keV. However, processes involving dust are complicated and all the calculations described have been carried out with assumptions about the dust size distribution and composition. Uncertainties in these calculations and our application of them are probably large enough to account for factors of a few, and prevent us from ruling out this process as an important contribution to the X-ray emission in Tycho. Nevertheless it is clear that a relatively large mass of dust is required if dust fluorescence is important.

We have assumed that any dust present in the remnant is behind the blast wave. The presence of a significant amount of dust in the ejecta may provide the mass of dust required by the X-ray data. Certainly, the ASCA Fe K images suggest that the Fe K line emission is distributed radially interior to the other emission lines, which would support its origin in ejecta. However, there are reasons to believe that most of the IR-emitting dust in the remnant is from shocked interstellar material. The IR radial profiles peak at radii outside the X-ray and radio radial profiles, which are both bright in emission from the reverse shock through the ejecta (Braun 1987); this suggests that most of the IR emission is from the blast wave. Hamilton & Fesen (1988) argue that the relatively low ratio of X-ray to IR luminosity in SN1006 implies that there cannot be a large quantity of dust in the remnant; Tycho’s SNR has a similar X/IR luminosity ratio, so a similar argument would apply. These considerations, in combination with the expectation from the ASCA Fe K image that the Fe K emission is primarily from the ejecta suggests that the dust fluorescence scenario probably cannot be the primary explanation for the discrepancy in Fe L/K intensities in the two-temperature models of Section 2.1. Nevertheless, since dust is present in Tycho’s SNR, one may expect that the process described here does occur.

### 3. Discussion

The ejecta plus blast emission model of Section 2.2 makes certain predictions about the relative strength of the various spectral components that can be compared to available imaging data. Seward et al. (1983) estimate that 28% of the count rate at energies 0.5–4.5 keV in the Einstein High Resolution Imager (HRI) is due to emission from the blast wave. By folding our model through the Einstein HRI response we find that a comparable fraction (32%) of the counts in the HRI band is due to the blast wave component.

We also consider the ASCA emission line images presented by HG97. The Fe K radial profile peaks at a smaller radius than the other ASCA images, including the adjacent 4–6 keV continuum and the Fe L emission at 1 keV. This is evident in the radial profiles shown in Figure 9 of HG97. The Fe K image is made up of continuum emission from the blast wave, plus line emission from both the blast wave and the ejecta. Since the 4–6 keV continuum image is dominated by the blast wave emission, we assume that the continuum contribution to the Fe K image has the same spatial distribution. We can then subtract the blast wave contribution to the Fe K image by scaling the 4–6 keV radial profile to the Fe K radial profile at the outermost radii, where the ejecta should make little or no contribution to the count rate. Subtracting this contribution from the total leaves about 32% of the Fe K image from the Fe ejecta. Our spectral model with the Fe ejecta at 4.0 keV predicts that this fraction is  $\sim 40\%$ , which is in reasonable agreement considering that these calculations are only intended to be illustrative. The spatial distribution of the Fe L emission is consistent with its origin being predominately in the blast wave, as it is in our model.

The ejecta models for Tycho provide satisfactory fits overall, but still slightly underestimate the Fe K flux by about 10%. The deficit is comparable to the contribution of the blast wave to the Fe K line emission. Although we have argued that dust fluorescence is not the dominant contribution to the Fe K line emission, it is certainly possible that dust in the swept-up interstellar medium would contribute an extra factor of two to the Fe K flux of the blast-wave component. The dust contribution would be at an energy of about 6.40 keV. Depletion of interstellar material onto dust grains would also explain why the fitted abundances in the blast wave component are sub-solar. It is also possible that a more sophisticated hydrodynamic scenario is required; certainly all real remnants have complex temperature, abundance, and density distributions that will manifest themselves given sufficiently high quality data.

In our analysis, we have purposely focused on the data from the best-calibrated chip of the SIS for technical reasons. The temperature of the gas in Tycho is certainly not uniform across the face of the remnant, as the results of HG97 show. However, the temperature variations to which the ASCA data are sensitive are relatively modest (roughly 50%), and the reader is referred to HG97 for a discussion of the variation of the spectrum with position in the remnant.

Our analysis indicates that the blast wave temperature  $kT$  in Tycho’s SNR is from a few to several keV. High energy flux has been detected from the remnant by HEAO-1 (Pravdo & Smith 1979) and Ginga (Fink et al. 1994). Fink et al. present spectral fits to the spectrum

at energies above 5 keV which require two components. One is a thermal component with temperature  $kT$  about 3 keV, which is in agreement with our blast wave component. Fink et al. conclude that the second, harder component could be either a hotter thermal component or a nonthermal component, but could not constrain the parameters for either. If our analysis is correct, then it is suggestive that the harder component measured by Fink et al. corresponds to nonthermal X-ray emission such as was observed in SN1006 (Koyama et al. 1995). If part of the continuum does come from such a nonthermal component, the derived abundances of the elements must be increased, since abundances are determined by the strength of the line emission relative to the thermal continuum. We have found that it is possible to hide a nonthermal X-ray source underneath the brighter thermal X-ray emission in the ASCA spectrum of Tycho with an unabsorbed luminosity at energies 0.5–10 keV on the order of  $10^{34}$  ergs  $s^{-1}$ . This is about an order of magnitude lower than the luminosity of the nonthermal component in SN1006. The nature of the high energy emission from Tycho’s SNR is an issue that will be of great interest to address with the spectral instruments on the X-ray Timing Explorer, which have sensitivity above 10 keV, where the second, harder component of Fink et al. begins to dominate.

We leave comparison of the data to a detailed hydrodynamical simulation to others, but consider briefly what initial density profiles for the ejecta may give rise to the observed temperature and ionization age structure. The power-law ejecta profiles described with similarity solutions by Chevalier (1982) give precisely the opposite trends in temperature and density as observed. Assuming that the Fe ejecta are interior to a mixed layer of lighter elements, the initial power-law density profile in the ejecta would imply higher density and lower temperature at inner radii. The constant density ejecta profiles described by Hamilton et al. (1986) do give a decrease in density with decreasing radius, as required, but do not give an increase in temperature because of the nonequilibrium of the electron temperature. This model predicts an expansion rate of the remnant that is higher than that measured in the radio, but consistent with recent X-ray measurements (Hughes 1996). A promising possibility is the exponential ejecta density profile, which appears to be a better description of Type Ia ejecta density profiles inferred from the modelling of SN. Although this model predicts a relatively flat temperature profile and decreasing density profile, the presence of a small amount of circumstellar matter may increase both the density and temperature contrast (Dwarkadas & Chevalier 1997).

#### 4. Summary and Conclusions

A spectral model with three separate constant temperature and ionization age NEI components provides a satisfactory fit to the ASCA SIS spectrum. This model makes no assumptions about the hydrodynamic structure of the remnant. One component representing ejecta is included at the temperature  $kT$  of 0.86 keV obtained by HG97 from analysis of line intensity ratios. The abundances of the intermediate mass elements in this component are in good qualitative agreement with those in Nomoto et al.’s (1984) W7 model for Type Ia supernovae.

The low fitted abundance of Fe relative to Si suggests that much of the Fe ejecta in Tycho’s SNR are spatially separated from the Si ejecta. A homogeneous distribution is not possible given the large mass of Fe ejecta expected in Type Ia remnants. This is in accordance with previously accumulated evidence (especially Hamilton, Sarazin, & Szymkowiak 1986) and with expectations from theory. The model therefore includes an additional component to represent Fe ejecta. The blast wave is modelled as a third component with its element abundances in the solar ratio.

The Fe L emission is relatively weak, and as noted, little of it is associated with the Si and other ejecta. The Fe K emission is prominent, but does not come primarily from either the Si ejecta component, which has too low a temperature, or the blast wave component. Most of the Fe K emission comes from Fe ejecta component, at a temperature at least twice that of the Si ejecta, and an ionization age about 100 times lower. A slight residual deficiency in the model Fe K flux may be explained by fluorescent emission from the dust in the remnant, or possibly by the complex hydrodynamic structure of the remnant. The model is consistent with the currently available imaging results.

Although fluorescent Fe K emission from dust can also qualitatively explain the Fe L/Fe K intensity ratio and Fe K centroid energy in Tycho, the mass of dust required to reproduce the Fe K intensity is very high compared to the dust mass estimates from IRAS observations. It cannot be ruled out, given the physical complexity of the process (a detailed comparison to the data would be required), but we believe that it is not likely to be the most important effect.

Our results leave some questions that will require more sophisticated modelling for their resolution. These include the slight residual deficiency in the Fe K blend and the issues of dust depletion of the elements in the interstellar medium and of a nonthermal X-ray component in the spectrum.

The authors thank Kazik Borkowski, Vikram Dwarkadas, Eli Dwek, Eric Gotthelf, and Andy Szymkowiak for profitable scientific discussions. We also express appreciation for the late Tom Markert, who provided input and encouragement. UH acknowledges support from an NRC research associateship. JPH acknowledges support from NASA grant NAG 5-4794.

Table 1. NEI Fits for  $E > 4.5$  keV

Blast $kT$ (keV)	$\chi^2$ ( $\nu=27$ )	Fe <sup>a</sup> (rel $\odot$ )	$\log \tau$ ( $\text{cm}^{-3} \text{ s}$ )	EM <sup>b</sup> ( $10^{12} \text{ cm}^{-5}$ )
2.5	22.0	3.4 (1.9–8.4)	10.12	8.3
3.0	19.4	3.1 (1.8–6.7)	10.07	6.1
3.3	18.0	2.9 (1.8–5.3)	10.06	5.0
4.0	17.2	2.6 (1.6–4.8)	10.03	3.9
4.5	16.9	2.5 (1.5–4.2)	10.03	3.5
5.0	17.1	2.4 (1.4–4.0)	10.02	3.1
6.0	17.4	2.2 (1.4–3.6)	10.02	2.7
7.0	18.3	2.1 (1.3–3.4)	10.02	2.4
10.0	20.3	1.9 (1.2–2.9)	10.03	2.0
20.0	24.2	1.6 (1.0–2.3)	10.10	1.8

<sup>a</sup>Abundances are relative to assumed solar value of  $3.98 \times 10^{-5}$  relative to H by number (Allen 1973). The range in parentheses corresponds to  $\Delta\chi^2 = 2.71$ .

<sup>b</sup>Emission measures should be scaled by  $\sim 2.3$  to normalize to the entire remnant.

TABLE 2  
TWO-COMPONENT NEI FIT RESULTS<sup>a</sup>

kT <sub>2</sub> (keV)	$\chi^2$ ( $\nu = 144$ )	N <sub>H</sub> (10 <sup>22</sup> cm <sup>-2</sup> )	log n <sub>e</sub> t <sub>1</sub> (cm <sup>-3</sup> s)	Si <sub>1</sub> (rel ☉)	Fe <sub>1</sub> (rel ☉)	EM <sub>1</sub> <sup>b</sup> (10 <sup>12</sup> cm <sup>-5</sup> )	log n <sub>e</sub> t <sub>2</sub> (cm <sup>-3</sup> s)	Fe <sub>2</sub> (rel ☉)	EM <sub>2</sub> <sup>b</sup> (10 <sup>12</sup> cm <sup>-5</sup> )
2.5	245.9	0.59	11.06	53	0.76	2.08	10.06	0.17	7.56
3.0	235.2	0.58	11.08	32	0.44	3.38	10.06	0.21	6.01
3.1	233.9	0.57	11.08	32	0.44	3.37	10.07	0.21	5.81
3.2	232.9	0.57	11.08	32	0.43	3.36	10.08	0.22	5.61
3.3	232.5	0.58	11.09	29	0.39	3.75	10.06	0.24	5.39
3.4	232.1	0.58	11.09	29	0.39	3.74	10.07	0.25	5.23
3.5	231.9	0.57	11.09	29	0.37	3.73	10.08	0.25	5.08
3.6	231.8	0.57	11.09	29	0.37	3.74	10.08	0.26	4.94
3.7	231.9	0.57	11.10	29	0.37	3.74	10.09	0.27	4.81
3.8	232.1	0.56	11.10	29	0.35	3.73	10.10	0.28	4.68
3.9	232.4	0.56	11.11	29	0.34	3.74	10.10	0.28	4.57
4.0	233.1	0.56	11.11	26	0.28	4.18	10.11	0.30	4.42
4.5	235.6	0.55	11.12	26	0.29	4.20	10.11	0.32	4.01
5.0	239.5	0.55	11.13	26	0.29	4.21	10.11	0.35	3.70
7.0	243.8	0.57	11.10	11	0.10	10.2	10.13	0.51	2.74
10.0	252.0	0.57	11.10	8.6	0.08	12.6	10.15	0.63	2.29
15.0	260.8	0.57	11.10	7.1	0.07	15.0	10.15	0.67	2.08
20.0	266.7	0.58	11.09	6.7	0.07	15.8	10.20	0.74	1.97

<sup>a</sup>kT<sub>1</sub> = 0.86 keV

<sup>b</sup>Emission measures should be scaled by  $\sim 2.3$  to normalize to the entire remnant.

TABLE 3  
TWO-COMPONENT NEI FIT RESULTS WITH ADDITIONAL FE<sup>a</sup>

$kT_{Fe}$ (keV)	$\chi^2$ ( $\nu = 142$ )	$N_H$ ( $10^{22}$ cm $^{-2}$ )	$\log n_e t_1$ (cm $^{-3}$ s)	Si <sub>1</sub> (rel $\odot$ )	Fe <sub>1</sub> (rel $\odot$ )	EM <sub>1</sub> <sup>b</sup> ( $10^{12}$ cm $^{-5}$ )	$\log n_e t_{Fe}$ (cm $^{-3}$ s)	EM <sub>Fe</sub> <sup>b</sup> ( $10^{12}$ cm $^{-5}$ )	$\log n_e t_2$ (cm $^{-3}$ s)	Z <sub>2</sub> (rel $\odot$ )	EM <sub>2</sub> <sup>b</sup> ( $10^{12}$ cm $^{-5}$ )
1.0	210.1	0.59	11.12	35	0	3.08	9.02	571	10.27	0.45	4.16
1.3	198.3	0.59	11.11	37	0.10	2.93	9.00	821	10.25	0.44	3.73
1.4	196.7	0.58	11.12	34	0.15	3.22	9.00	643	10.23	0.40	3.76
1.5	196.1	0.58	11.12	33	0.13	3.29	9.01	468	10.23	0.40	3.84
1.6	196.1	0.58	11.13	33	0.12	3.29	9.02	340	10.24	0.40	3.92
		(0.54–0.61)	(11.09–11.16)	(31–35)	(<0.6)		(<9.04)		(10.03–10.28)	(0.25–0.51)	
1.7	196.4	0.58	11.13	33	0.10	3.28	9.03	256	10.24	0.40	3.97
1.8	196.6	0.58	11.13	33	0.08	3.29	9.04	190	10.25	0.41	4.03
1.9	196.8	0.58	11.13	32	0.07	3.36	9.05	150	10.25	0.41	4.06
2.0	197.0	0.58	11.14	33	0.06	3.34	9.07	120	10.25	0.41	4.09
2.5	197.0	0.57	11.14	32	0.06	3.36	9.18	54	10.25	0.40	4.16
3.0	196.9	0.57	11.14	32	0.04	3.42	9.23	30	10.25	0.40	4.20
3.5	196.8	0.57	11.14	31	0.04	3.52	9.27	20	10.25	0.40	4.21
4.0	196.6	0.57	11.14	34	0.04	3.53	9.30	16	10.25	0.40	4.21
5.0	196.1	0.57	11.14	34	0.05	3.53	9.39	11	10.25	0.39	4.23
6.0	195.7	0.57	11.14	34	0.02	3.57	9.46	7.3	10.26	0.39	4.26
7.0	195.5	0.57	11.14	33	0.02	3.58	9.49	6.3	10.25	0.39	4.26
10.0	194.7	0.57	11.14	30	0	3.64	9.64	4.07	10.26	0.38	4.28
15.0	194.3	0.56	11.13	28	0	3.83	9.78	3.07	10.27	0.36	4.28
20.0	194.2	0.55	11.13	28	0	3.91	9.85	2.81	10.27	0.33	4.28

<sup>a</sup> $kT_1 = 0.85$  keV,  $kT_2 = 4.0$  keV

<sup>b</sup>Emission measures should be scaled by  $\sim 2.3$  to normalize to the entire remnant.

Table 4. Fe Masses

Blast $kT$ (keV)	$M_{\text{Fe}}$ ( $M_{\odot}$ ) (gas + dust) <sup>a</sup>	$M_{\text{Fe}}$ ( $M_{\odot}$ ) gas	$M_{Fe}$ ( $M_{\odot}$ ) dust
2.5	0.018	0.0011	0.017
3.0	0.013	0.0012	0.012
3.3	0.011	0.0012	0.010
4.0	0.009	0.0014	0.007
5.0	0.007	0.0015	0.006
6.0	0.006	0.0017	0.005
7.0	0.005	0.0017	0.004
10.0	0.004	0.0017	0.002

<sup>a</sup>Using BS97 for  $\log n_e t$  ( $\text{cm}^{-3} \text{s}$ ) = 10.3

## REFERENCES

- Albinson, J. S., Tuffs, R. J., Swinbank, E., & Gull, S. F. 1986, MNRAS, 219, 427
- Allen, C. 1973, *Astrophysical Quantities*
- Borkowski, K., & Szymkowiak, A. E. 1996, ApJ, 477, L49
- Branch, D., Doggett, J. B., Nomoto, K., & Thielemann, F.-K. 1985, ApJ, 294, 619
- Braun, R. 1987, A&A, 171, 233
- Chevalier, R. A. 1982, ApJ, 258, 790
- Dwarkadas, V. V., & Chevalier, R. A. 1997, ApJ, submitted
- Fink, H. H., Asaoka, I., Brinkmann, W., Kawai, N., & Koyama, K. 1994, A&A, 283, 635
- Green, D. A. 1984, MNRAS, 209, 449
- Hamilton, A. J. S., & Fesen, R. A. 1988, ApJ, 327, 178
- Hamilton, A. J. S., & Sarazin, C. L. 1984, ApJ, 284, 601
- Hamilton, A. J. S., & Sarazin, C. L., & Chevalier, R. A. 1983, ApJS, 51, 115
- Hamilton, A. J. S., Sarazin, C. L., & Szymkowiak, A. E. 1986, ApJ, 300, 713
- Hughes, J. P. 1991, *Supernovae*, ed. Woosley, S. E. (New York: Springer Verlag), 661
- Hughes, J. P. 1996, *X-ray Imaging and Spectroscopy of Cosmic Hot Plasmas*, (Tokyo: Universal Academy Press), 359
- Hughes, J. P., & Helfand, D. J. 1985, ApJ, 291, 544
- Hughes, J. P., & Singh, K. P. 1994, ApJ, 422, 126
- Hwang, U., & Gotthelf, E. V. 1997, ApJ, 475, 665
- Hwang, U., Hughes, J. P., Canizares, C. R., & Markert, T. H. 1993, ApJ, 414, 219
- Kirshner, R., Winkler, P. F., & Chevalier, R. A. 1987, ApJ, 315, L135
- Koyama, K., Petre, R., Gotthelf, E. V., Hwang, U., Matsuura, M., Ozaki, M., & Holt, S. S. 1995, Nature, 378, 255
- Liedahl, D. A., Osterheld, A. L., & Goldstein, W. H. 1995, ApJ, 438, L115
- Mewe, R., Gronenschild, E. H. B. M., & van den Oord, G. H. J. 1985, A&AS, 62, 197
- Nomoto, K., Thielemann, F.-K., & Yokoi, K. 1984, ApJ, 286, 644
- Petre, R., *et al.* 1992, *UV and X-ray Spectroscopy of Laboratory and Astrophysical Plasmas*, ed. Silver, E., & Kahn, S. (Cambridge: Cambridge University Press), 424
- Pravdo, S. H., & Smith, B. W. 1979, ApJ, 234, 195L
- Raymond, J. C., & Smith, B. W. 1977 ApJS, 35, 419

- Reynolds, S. R., Moffett, D. A., Goss, W. M., Reynoso, E., Dubner, G., & Dickel, J. 1996, BAAS, 189, 4608
- Seward, F. D., Gorenstein, P., & Tucker, W. 1983, ApJ, 266, 287
- Smith, R. C., Kirshner, R. P., Blair, W. P., Winkler, P. F 1991, ApJ, 375, 652
- Thielemann, F.-K., Nomoto, K., & Hashimoto, M. 1993, Origin and Evolution of the Elements (Cambridge: Cambridge University Press), 297
- Vancura, O., Gorenstein, P., & Hughes, J. P. 1995, ApJ, 441, 680
- Woosley, S., ed. 1991, Supernovae (Berlin: Springer-Verlag)
- Wu, C.-C., Crenshaw, D. M., Fesen, R. A., Hamilton, A. J. S., & Sarazin, C. L. 1993, ApJ, 416, 247
- Wu, C.-C., Crenshaw, D. M., Hamilton, A. J. S., Fesen, R. A., Leventhal, M. & Sarazin, C. CL. 1997, ApJ, 477, L53
- Wu, C.-C., Leventhal, M., Sarazin, C. L., & Gull, T. R. 1983, ApJ, 269, L5

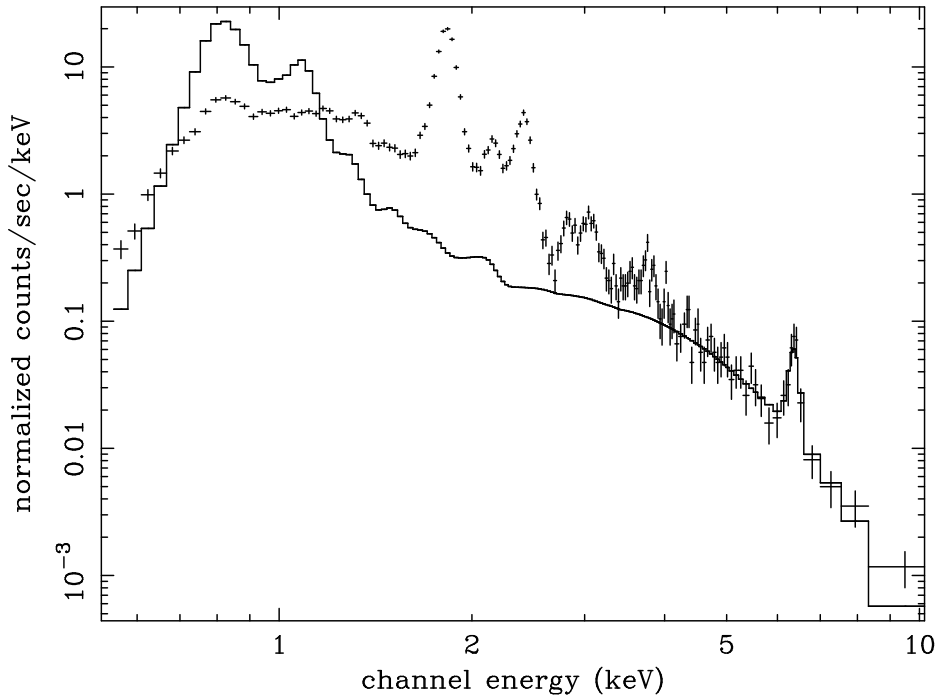


Fig. 1.— The ASCA (SIS0, chip 1) spectrum of Tycho’s SNR overlaid with the best-fit NEI model for continuum and Fe, fitted at energies above 4.5 keV and extrapolated to lower energies. The Fe L emission is severely overpredicted, even in the absence of the ejecta component required to explain the strong Si and S line emission at 1.86 and 2.45 keV. The model assumes the Galactic column density of  $4.5 \times 10^{21} \text{ cm}^{-2}$  and is folded through the instrument response.

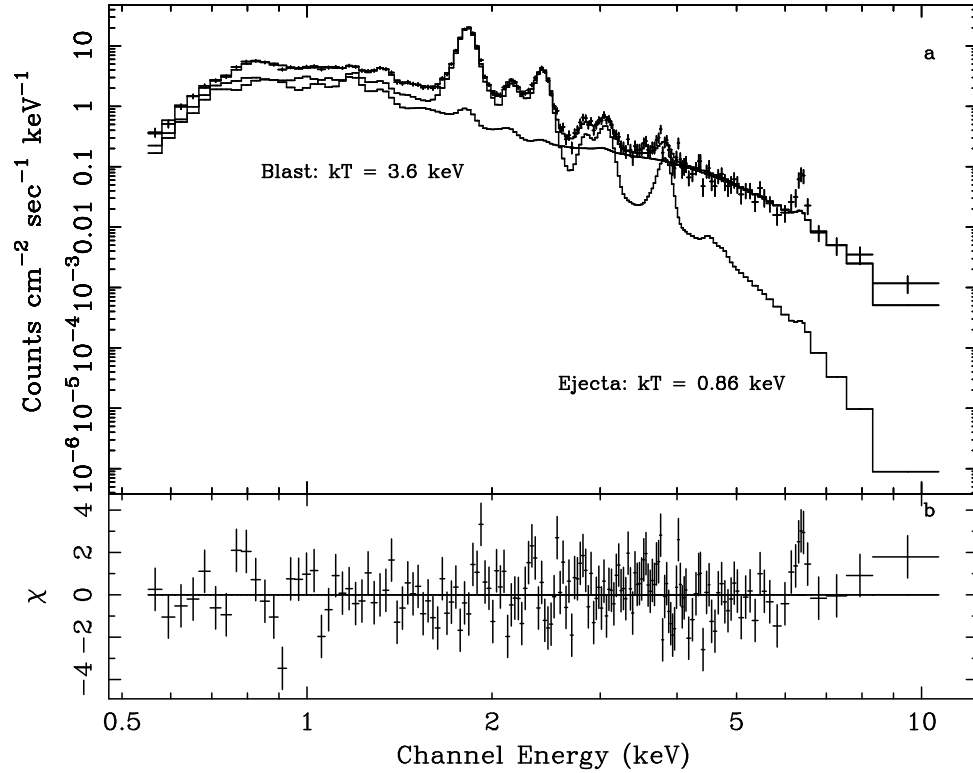


Fig. 2.— The data overlaid with the two temperature NEI model with ejecta temperature  $kT = 0.86$  keV and blast temperature  $kT = 3.6$  keV (the model with the lowest formal  $\chi^2$ ). The lower panel shows the residuals. The contribution of each component is shown separately. The ejecta component can be recognized as it contributes most of the strong Si and S emission, while the blast component provides most of the continuum at energies above 5 keV. This model, constrained by the Fe L emission, provides insufficient emission in the Fe K blend at  $\sim 6.5$  keV.

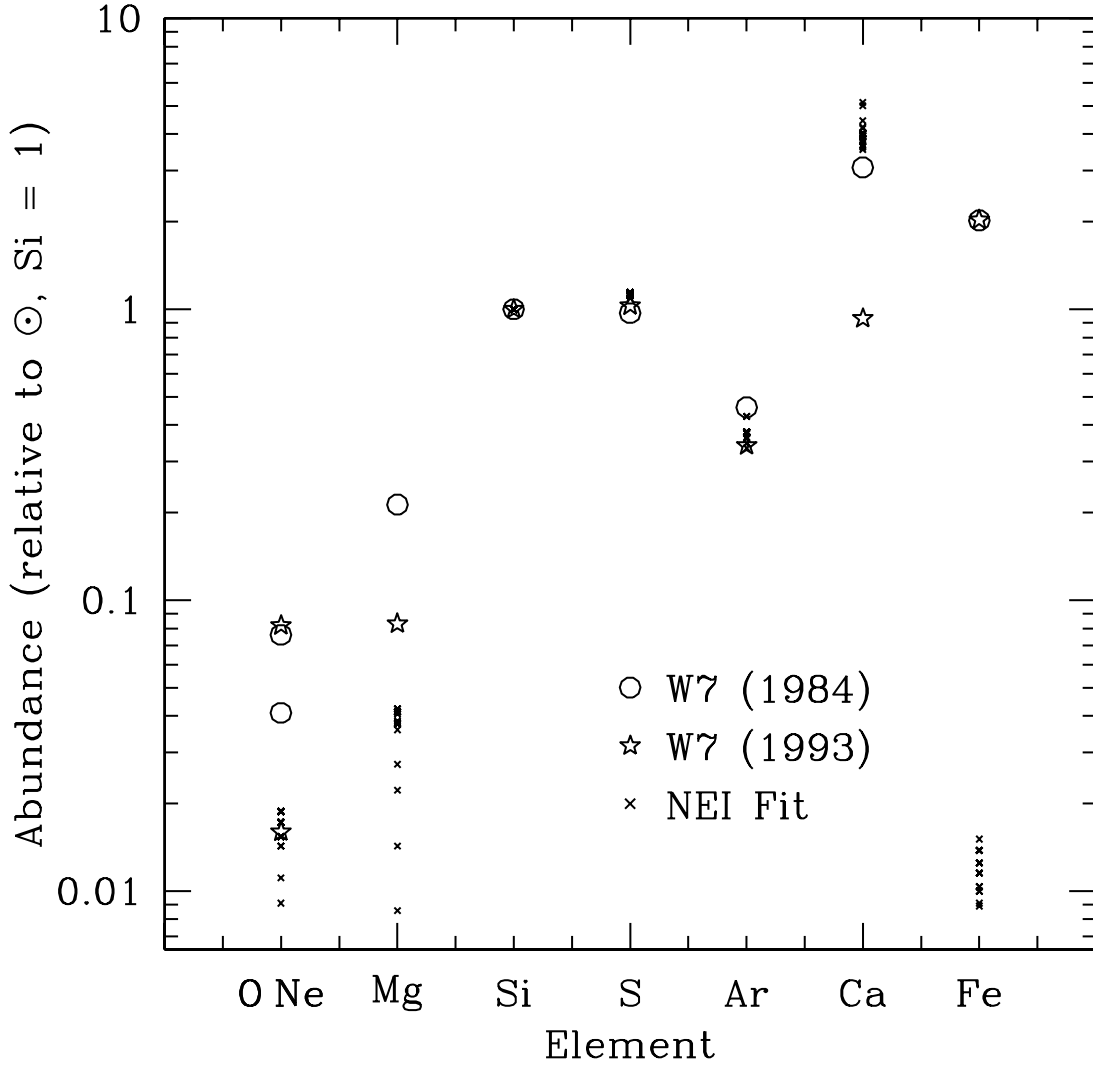


Fig. 3.— The abundances of the elements relative to Si, relative to the solar values of Allen (1973) from the fits in Table 2. Also shown are the abundances calculated for the W7 model for a Type Ia supernova by Nomoto et al. (1984) and the updated calculations by Thielemann et al. (1993). O and Ne are shown in the same column; in both models, the Ne abundance is lower than the O abundance.

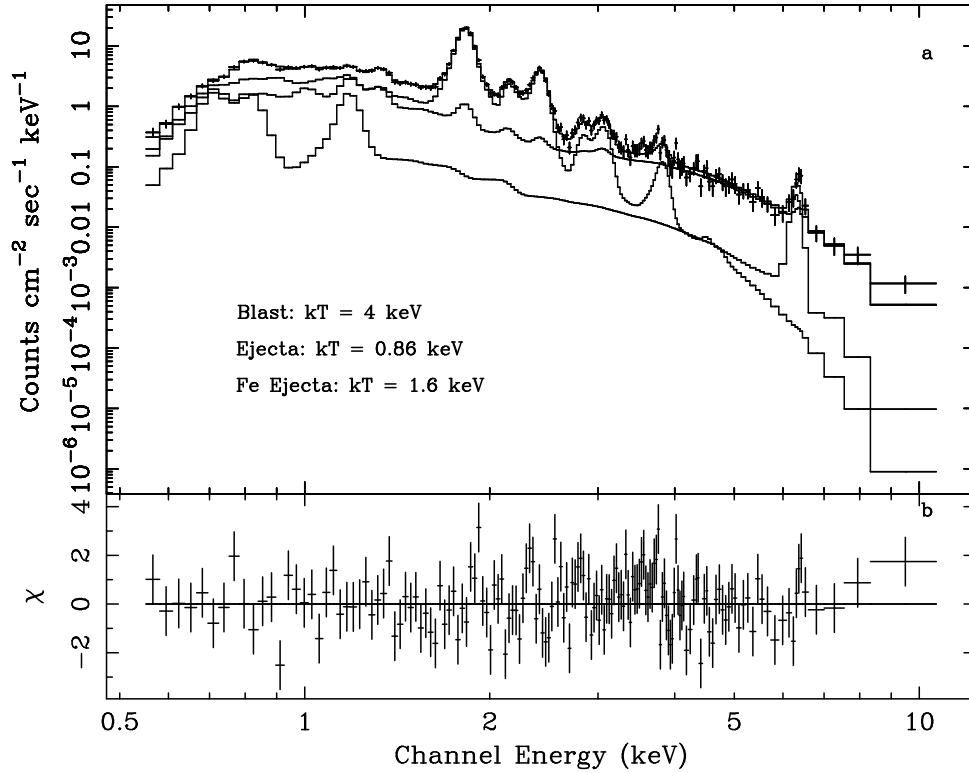


Fig. 4.— The data overlaid with the NEI model with ejecta at temperature  $kT = 0.86$  keV, additional Fe ejecta at temperature  $kT = 1.6$  keV, and blast component at temperature  $kT = 4$  keV, folded through the instrument response. The lower panel shows the residuals. The contribution of each component is shown separately. The ejecta component can be recognized as it contributes most of the strong Si and S emission, while the blast component provides most of the continuum at energies above 5 keV. The curves for the ejecta and blast wave cross at about 1.2 keV.